Atmospheric Environment 119 (2015) 348–361

Contents lists available at ScienceDirect

Atmospheric Environment

journal homepage: www.elsevier.com/locate/atmosenv

Smoke dispersion modeling over complex terrain using high resolution meteorological data and satellite observations – The FireHub platform

S. Solomos [a, *], V. Amiridis [a], P. Zanis [b], E. Gerasopoulos [c], F.I. Sofiou [a], T. Herekakis [a], J. Brioude [d, e], A. Stohl [f], R.A. Kahn [g], C. Kontoes [a]

[a] Institute for Astronomy, Astrophysics, Space Applications and Remote Sensing, National Observatory of Athens, Athens, Greece
[b] Department of Meteorology and Climatology, School of Geology, Aristotle University of Thessaloniki, University Campus, Thessaloniki, Greece
[c] Institute for Environmental Research and Sustainable Development, National Observatory of Athens, Greece
[d] Chemical Sciences Division, Earth System Research Laboratory, NOAA, Boulder, CO 80305, USA
[e] Cooperative Institute for Research in Environmental Sciences, University of Colorado, Boulder, CO 80309, USA
[f] Department for Atmospheric and Climate Research, Norwegian Institute for Air Research, Kjeller, Norway
[g] NASA Goddard Space Flight Center, Greenbelt, MD, USA

HIGHLIGHTS

- A synergistic satellite-modeling approach is proposed for biomass smoke forecasts.
- FLEXPART-WRF model allows the description of biomass dispersion at local scale.
- Satellite data (MISR, MODIS, SEVIRI) are used to constrain and evaluate the model.
- Interchange between marine and land PBL affects smoke plume properties.
- Satellite FRP is necessary for the top-down estimation of emissions and plume rise.

ARTICLE INFO

Article history:
Received 26 June 2015
Received in revised form
20 August 2015
Accepted 21 August 2015
Available online 24 August 2015

Keywords:
Fire smoke
Injection height
Smoke dispersion modeling
FireHub

ABSTRACT

A total number of 20,212 fire hot spots were recorded by the Moderate Resolution Imaging Spectroradiometer (MODIS) satellite instrument over Greece during the period 2002–2013. The Fire Radiative Power (FRP) of these events ranged from 10 up to 6000 MW at 1 km resolution, and many of these fire episodes resulted in long-range transport of smoke over distances up to several hundred kilometers. Three different smoke episodes over Greece are analyzed here using real time hot-spot observations from the Spinning Enhanced Visible and Infrared Imager (SEVIRI) satellite instrument as well as from MODIS hot-spots. Simulations of smoke dispersion are performed with the FLEXPART-WRF model and particulate matter emissions are calculated directly from the observed FRP. The modeled smoke plumes are compared with smoke stereo-heights from the Multiangle Imaging Spectroradiometer (MISR) instrument and the sensitivities to atmospheric and modeling parameters are examined. Driving the simulations with high resolution meteorology (4 × 4 km) and using geostationary satellite data to identify the hot spots allows the description of local scale features that govern smoke dispersion. The long-range transport of smoke is found to be favored over the complex coastline environment of Greece due to the abrupt changes between land and marine planetary boundary layers (PBL) and the decoupling of smoke layers from the surface.

1. Introduction

Emissions of smoke from open biomass burning (BB) are an important feature of the Earth system as they include numerous gas and aerosol species (e.g. Andreae and Merlet, 2001), many of them

* Corresponding author.
E-mail address: stavros@noa.gr (S. Solomos).

http://dx.doi.org/10.1016/j.atmosenv.2015.08.066
1352-2310/

associated with climate change. The contribution of BB to global emissions into the atmosphere has been estimated to be about 40% for carbon monoxide (CO), 35% for carbonaceous particles, and 20% for nitrogen oxides (NOx) (Langmann et al., 2009). According to most climate change scenarios (IPCC, 2014) the number of large fires worldwide is expected to increase in the coming decades. In this context the effects of BB emissions on weather and climate need to be carefully assessed. Emissions of gases such as CO, CO_2 and CH_4 have long been associated with climate change, but significant uncertainty remains regarding the role of black carbon (BC) and organic carbon (OC) aerosols in the atmosphere. Smoke aerosols affect radiative transfer (e.g. Andreae, 1993; Nenes and Seinfeld, 2003; Myhre et al., 2013), serve as Cloud Condensation Nuclei (CCN) and ice nuclei (IN) affecting the formation of clouds (e.g. Brioude et al., 2009), and may have an influence on hazardous weather events, such as tornadogenesis (Saide et al., 2015). The net effect of BB emissions on climate change becomes even more uncertain when the change in surface albedo from the deposition of BC on ice and snow and the decline of sensible heat flux over the burned area that persists for decades (Randerson et al., 2006) are taken into account. The overall uncertainty in the composition and magnitude of the BB aerosol emissions in climate models makes the quantification of BB net radiative forcing uncertain as well (Petrenko et al., 2012; Myhre et al., 2013) and emphasizes on the need for a more accurate representation of smoke emissions and dispersion in relevant modeling studies.

Apart from the atmospheric forcing, smoke emissions from both agricultural and forest fires deteriorate air quality and can result in serious health hazards (e.g., Stohl et al., 2007; Liu et al., 2009). The principal health threat related to BB smoke is the possible inhalation of smoke particulate matter (PM) since the smoke particles are usually within the fine particle size range (PM2.5). The exact composition of smoke and the total PM emissions depend on the fuel type, fuel moisture and also the fire stage (flaming or smoldering). In Europe, more than 50,000 fire episodes per year result in about 5000 km^2 of burned forests (Keramitsoglou et al., 2004). Although this is much less than for example in Asia or North America, these fires are still important because of the high population density in Europe. Vegetation fires are also significantly contributing to trans-boundary pollution (e.g. Amiridis et al., 2009). In general, intense fire events that last for several days are capable of producing elevated smoke plumes that can travel over thousands of kilometers (Forster et al., 2001; Colarco et al., 2004). The fate of smoke plumes in the atmosphere is determined by the initial properties of the fire itself (i.e. fuel type, load, and moisture, pyrocumulus convection, injection height) and by the local and regional atmospheric conditions (atmospheric stability, mixing layer depth, wind shear, etc.)

Emissions of smoke in dispersion models are often estimated on the basis of fire "hot spots" detections by satellite instruments. Space-borne instruments onboard geostationary and polar orbiting satellites can provide valuable information for real time fire detection systems and for event analysis studies. However, fire detection alone is not sufficient for determining the emission flux, as this depends on the severity of fire, type of biomass, etc. For the computation of injection heights, several parameterizations have been proposed based on fire properties, burning fuel and meteorological conditions. Most of these algorithms rely on the Fire Radiative Power (FRP) as a representative macroscopic measure of fire intensity (Wooster et al., 2005; Ichoku and Kaufman, 2005; Freitas et al., 2007; Sofiev et al., 2009) and on atmospheric modeling techniques that solve smoke dispersion equations (Brioude et al., 2009; Athanasopoulou et al., 2014; Saide et al., 2015). Proper handling of atmospheric dynamics is particularly critical for short-term forecasts since a minor misrepresentation in modeled wind shear can result in a discrepancy of many kilometers between the forecasted and the actual plume downwind of the source.

Currently, the ability of the MISR instrument to observe both smoke plume heights and horizontal plume dimensions is the closest we can get to real-time observations of smoke plume structure. However, since it takes about a week for MISR to obtain global coverage, it can only contribute a snapshot of an eitherwise rapidly evolving phenomenon, provided that it is coincidentally captured by an overpass and this has happened under cloud-free conditions. Few operational systems, that employ satellite data and modeling techniques, have been developed in Europe, based on different satellite platforms. For example, Kelha et al. (2003) describe a fire detection system for Finland based on AVHRR and AATSR instruments. Sofiev et al. (2009) also describe an operational air quality system over Europe including fire emissions based on MODIS satellite data and smoke dispersion calculations with the Eulerian chemical transport model SILAM (Sofiev et al., 2006). These systems rely on polar orbiting instruments to identify a fire spot, which limits the time resolution to the return periods of the satellites. All the above bring out the need to develop a physically based methodology for simulating smoke dispersion based on geostationary satellite data, which are available all the time. Along this line, the NAAPS system (Navy Aerosol Analysis and Prediction System, http://www.nrlmry.navy.mil/aerosol) provides smoke forecasts at a horizontal resolution of $1^\circ \times 1^\circ$ based on the WFABBA fire detections (Wildfire Automated Biomass Burning Algorithm, http://wfabba.ssec.wisc.edu/).

In this study, we utilize a synergistic satellite/modeling tool that has been developed at the National Observatory of Athens under the FireHub platform (http://ocean.space.noa.gr/fires), driven by geostationary observations from the MSG/SEVIRI instrument. The aim of the study is to articulate improvements in resolving and forecasting the dispersion of smoke plumes over the particularly complex terrain of Greece, by incorporating high-resolution (spatial and temporal) meteorology and satellite data.

2. Methodology

The efficiency of the operational BB smoke dispersion modeling system depends on the availability and quality of input data as well as on the ability to represent the local meteorological and fire emission properties. In this direction, several synergistic satellite and modeling tools have been developed in the frame of the FireHub integrated platform. The main components of this system are presented in the following sections.

2.1. Satellite observations

The precise location, ignition time and duration of wildfires is obtained online from the Meteosat Second Generations MSG/SEVIRI observations (Kontoes et al., 2013). FireHub is a real-time fire monitoring system that combines well-established generic tools and open standards for data modeling and representation in an innovative service chain. It is based on a modular architecture using MSG-SEVIRI sensor images acquired on a 5-min basis in conjunction with atmospheric modeling outputs from the Weather Research and Forecasting model (WRF). Earth Observation (EO) data are combined with ancillary landscape evidence and meteorological forecasts to derive reliable sub-pixel approximations of the position of the active hot spots in the MSG-SEVIRI pixel (Sifakis et al., 2011). FireHub is a downstream Copernicus service for crisis management related to fire and smoke episodes, and can be easily expanded to cover any area inside the MSG/SEVIRI disc. It is used on a 24/7 basis supporting the operations of the Disaster Control Room

of Fire Brigades in Greece. Within this context, the performance of the developed system has been validated against real wildfire data using the fire records of the Greek Fire Brigade Service. The use of geostationary satellite information at this high temporal resolution allows the description of the diurnal and short-term variability of the fire emissions. SEVIRI FRP retrievals are not yet implemented in FireHub and the FRP values are obtained from MODIS data (Terra and Aqua overpasses) as provided by the Fire Information for Resource Management System (FIRMS) database (https://earthdata.nasa.gov/active-fire-data).

Information on the elevation of smoke plumes is obtained from the multi-angle imaging spectroradiometer (MISR). MISR flies aboard the NASA Earth Observing System's Terra satellite and includes nine cameras viewing the Earth at different angles, with a swath width of about 380 km. This instrument has been designed for climate observations, specifically for long-term study of atmospheric aerosols, clouds, and land surface properties. Stereo-scopic viewing allows the acquisition of multiangle images of smoke, desert dust, and volcanic ash plumes, providing also information on the geometry of the plumes in both horizontal and vertical dimensions (Kahn et al., 2007). To obtain three-dimensional plume geometric properties, MISR images are processed with the MISR Interactive eXplorer (MINX) software (Nelson et al., 2008; 2013; Val Martin et al., 2010, 2012).

2.2. Smoke dispersion modeling

The satellite observations from SEVIRI, MODIS and MISR together with the atmospheric modeling data are used as inputs to the Lagrangian dispersion model FLEXPART-WRF (Brioude et al., 2013) for the description of BB smoke dispersion. FLEXPART-WRF simulations are driven by hourly meteorological outputs from the Weather Research and Forecasting (WRF) model. We use the WRF-ARW core (Skamarock et al., 2008) configured at a resolution of 12 × 12 km (external grid), 4 × 4 km (two-way nested inner grid) and 31 vertical levels as seen in Fig. 1a. Initial and boundary fields are from the NCEP final analysis dataset (FNL) at 1° × 1° resolution. Daily updated Sea Surface Temperature (SST) is taken from the NCEP 1° × 1° analysis.

The MODIS hot spots are obtained from the FIRMS database and the SEVIRI hot-spots from the FireHub platform. The amount of fuel consumed by the fire is related to the fire intensity, so it can be estimated directly from the FRP retrievals. For the computation of smoke emission rates, and in the context of limiting the need for additional information on fuel type and burned area, we have adopted the top-down approach proposed by Ichoku and Kaufman (2005). Following their approach, the smoke aerosol emission rates (E) are computed directly from satellite FRP observations as:

$$E\left(\text{kg s}^{-1}\right) = C\left(\text{kg MJ}^{-1}\right) \times FRP\left(\text{MJ s}^{-1}\right) \quad (1)$$

The advantage of this method is that emission rates are computed in real time and are directly linked to the intensity of the fire as observed by satellite instruments. For the Region of Interest (RoI), we use a value of C = 0.026 kg MJ^{-1} for the smoke aerosol emission coefficient, as derived from the global 1° × 1° top-down smoke aerosol emission coefficient database (http://feer.gsfc.nasa.gov/) developed by Ichoku and Ellison (2014).

For the computation of injection heights, the explicit plume rise parameterization of Freitas et al. (2007) has been implemented in the FLEXPART-WRF model, based on a previous implementation in the original FLEXPART model by Brioude et al. (2009). The plume rise parameterization is based on the assumption that FRP is proportional to fuel amounts and fire intensity (Wooster et al., 2005). For the computation of the sensible heat flux we assume that the radiative energy represents 10% of the total fire energy (Wooster et al., 2005; Freeborn et al., 2008). The vertical profiles of humidity and temperature are taken from the WRF hourly model outputs. For the current study, the plume rise scheme is employed only for runs that correspond to MODIS hot spots. Since a SEVIRI FRP product is not yet available for operational use, for the runs that are driven by SEVIRI hot spots, we assume a-posteriori prescribed

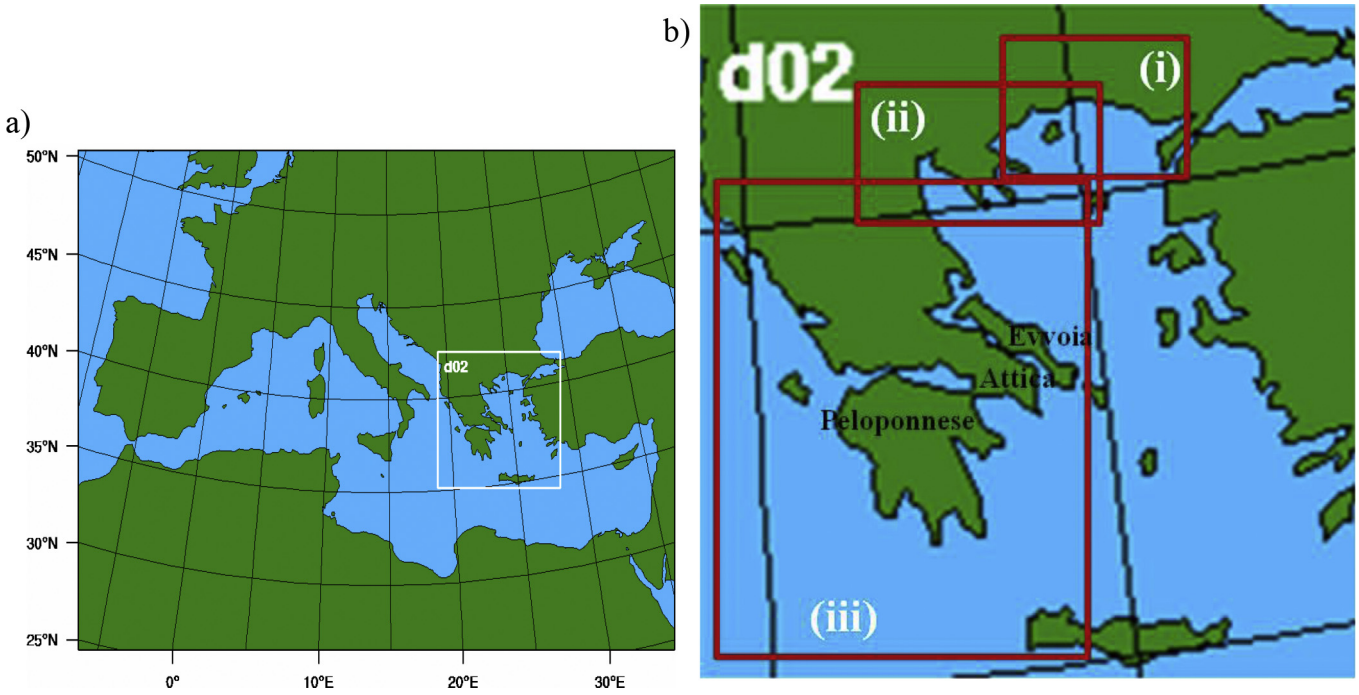

Fig. 1. a) WRF modeling domains. b) FLEXPART-WRF modeling domains for the three smoke episodes i) Evros, ii) Agion Oros iii) Peloponnese.

injection heights based on the MISR observations.

The coupling of FLEXPART with WRF eliminates the limitation of driving dispersion simulations only from the global ECMWF or GFS meteorology, and allows WRF-driven simulations of smoke dispersion at very high resolutions. In practice this means that FLEXPART-WRF can be applied at resolutions ranging from tens of kilometers down to several meters while standard FLEXPART-ECMWF and FLEXPART-GFS configurations normally rely on the $0.5^\circ \times 0.5^\circ$ global forecasting products. Moreover, the temporal resolution of WRF output fields can be also customized based on the simulation needs (e.g. use hourly wind fields instead of the three or six hourly products of the global models). This improvement is particularly important for areas like Greece that are characterized by complex topography and coastlines. Under such circumstances the increased mechanical mixing and the elevated sensible heat sources during daytime result in an accordingly complex spatial distribution of PBL heights – a feature that cannot be easily reproduced in mesoscale model resolutions.

For the Lagrangian simulations, a total of 10,000 particles are released for each fire hot spot and the modeling domains for the simulations of the current study are shown in Fig. 1b. The output domain in FLEXPART-WRF is set up with twenty vertical levels (250–5000 m by a 250 m step), and at a horizontal resolution of 4×4 km. The tracer particles are assumed to be smoke aerosol (total particulate matter – TPM). Smoke particles are usually very small (less than 1 μm in diameter) near the sources. However in order to account also for aging effects the simulated tracers are assumed to follow a mass size distribution with mean diameter of 2 μm and geometric standard deviation $\sigma = 2$ μm. Dry and wet removal processes are also enabled for these particles.

The offline coupling of the two models (WRF and FLEXPART) provides a computationally efficient solution for performing various sensitivity tests, serving also the need for real-time early warning system operations. In operational mode, the WRF simulations are performed once per day and provide 72 h forecast. These model files are then used to drive all subsequent smoke dispersion calculations. The five-minute intervals observations from the SEVIRI instrument are integrated into hourly emission files. The dispersion runs are initialized every hour and the model is set up to operate in warm–start cycle mode. Following this approach, each simulation takes into account the airborne smoke particles from the previous run. The advantage of this method is that the temporal variability of the smoke sources, as provided from the MSG/SEVIRI, is directly assimilated into the model.

3. Results

During the last decade, Greece has suffered a lot from devastating fires (Amiridis et al., 2012). Most severe fire events coincide with the strong north winds (etesians) during summer that constitute a major climatological component of the Aegean Sea (Tyrlis and Lelieveld, 2013). The depth of this flow can reach up to 3–4 km, with near surface speeds exceeding 20 m s^{-1} during daytime. Moreover, intense local thermal circulations (e.g. sea-breeze) occur during the warm period (July–August), in coincidence with the peak of the fire season. The above conditions result in amplification and uncontrollable spreading of the fires, which, in combination with the complex coastline and topography of Greece, create an ideal scene for the study of smoke dispersion and evaluation of forecast tools under rather challenging circumstances.

In this section, we present an analysis of MODIS FRP data over Greece and relevant fire smoke emissions in the RoI, while three case studies selected for their unique characteristics are further analyzed for evaluating the improvements in resolving and forecasting the dispersion of smoke plumes, by incorporating high-resolution (spatial and temporal) meteorology and satellite data.

3.1. Long term aspects of fire intensity and smoke emissions over Greece (2002–2013)

MODIS detected 20,212 fires in the RoI during the period 2002–2013. Colocation of the CORINE level_2 landuse types with the associated MODIS fire pixels indicates that 39% of the burning areas were scrub and/or herbaceous vegetation, 22% were heterogeneous agricultural areas, 17% were arable lands and 12% forests, with the remaining 10% being associated with different vegetation types. The FRP values range from less than 10 MW up to more than 6000 MW at 1 km resolution, indicating the large range of this parameter and the need to compute the fire intensity of each fire explicitly. More than half of the FRP observations (56%) are in the range between 10 and 50 MW, 19% lies between 50 and 100 MW and less than 1% are greater than 1000 MW. The latter, albeit low, corresponds to 202 satellite detections, and these intense fires make a disproportionate contribution to smoke emissions. The spatial distribution of the FRP values is presented in Fig. 2, where the majority of the fires with FRP >1000 MW are shown to be located in southern Evvoia, Attica and western Peloponnese. Amiridis et al. (2010) showed that the plumes crossing the Planetary Boundary Layer (PBL) into the free troposphere are the most likely to be transported over longer distances. The plumes that remain inside the PBL are well mixed and dissipate faster due to removal by dry deposition and the turbulence in the PBL that leads to a more rapid dilution. In this context, the smoke injection height relative to the PBL top is a major governing factor for long-range transport. In the following sub-sections, three characteristic events are analyzed and sensitivity tests are performed with the use of satellite (MISR, MODIS and SEVIRI) and modeling (FLEXPART, WRF) tools. The model configuration for each simulation and naming conventions are summarized in Table 1.

3.2. Case 1: typical fire event (Evros, 25 August 2011)

On 25 August 2011, at about 9:00 UTC, two distinct smoke plumes are identified by MISR in the area of Evros in northern

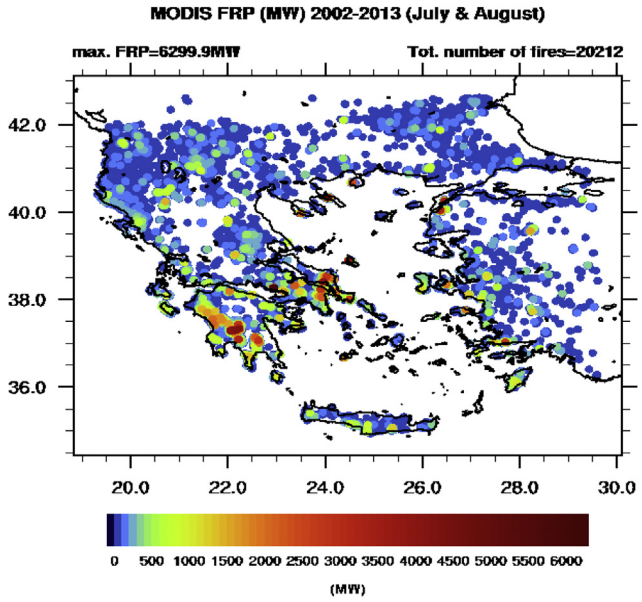

Fig. 2. Spatial distribution of July and August MODIS FRP values for the period 2002–2013.

Table 1
Model configuration for the smoke dispersion simulations.

Case study[a]	Fire hot spots	Meteorological input	Injection height
Evros_S4P	SEVIRI updated every hour (integrated 5 min detections)	WRF 4 × 4 km	Prescribed based on MISR heights
Evros_M4P	MODIS updated at every Terra or Aqua overpass[b]	WRF 4 × 4 km	Prescribed based on MISR heights
Evros_M4F	MODIS updated at every Terra or Aqua overpass	WRF 4 × 4 km	Calculated from MODIS FRP (Freitas plume rise scheme)
Agion_Oros_S4P	SEVIRI updated every hour (integrated 5 min detections)	WRF 4 × 4 km	Prescribed based on MISR heights
Agion_Oros_S50P	SEVIRI updated every hour (integrated 5 min detections)	WRF 50 × 50 km	Prescribed based on MISR heights
Agion_Oros_M4F	MODIS updated at every Terra or Aqua overpass	WRF 4 × 4 km	Calculated from MODIS FRP (Freitas plume rise scheme)
Peloponnese_S4P	SEVIRI updated every hour (integrated 5 min detections)	WRF 4 × 4 km	Prescribed based on MISR heights
Peloponnese_S50P	SEVIRI updated every hour (integrated 5 min detections)	WRF 50 × 50 km	Prescribed based on MISR heights

[a] Naming convention e.g. Evros_M4F stands for: Evros_MODIS_4 × 4 km_Freitas.
[b] About 1.5 h between Terra and Aqua and about 10 h between day and night overpasses.

Greece (Fig. 3a). The two plumes originate from two different fire events that started on the previous day and the horizontal distance between these two fires is about 6 km. The travel direction of the smoke is SW, towards the sea. At the time of Terra overpass (09:10 UTC), the smoke observed by the MISR instrument is up to 1 km close to the fires (i.e. injection height) and lifted up to 2 km downwind. The lowest and western parts of the plume are heavily dispersed along the coastline. As seen in Fig. 3b, this event is reproduced by the FireHub Evros_S4P simulation assuming a uniform release of particles from the surface up to 1000 m, as suggested by MISR observations. The modeling results indicate a wider dispersion of smoke near the sources (compared to the MISR image) and the simulated plume covers a longer distance towards SW. However, the main properties of the smoke dispersion, like the two distinct plumes, are reproduced in the model. The eastern plume is in general characterized by more elevated smoke and the western plume is quickly dispersed to the west just after reaching the coastline. The colocation of Evros_S4P simulated smoke with MISR plumes for this event is shown in Fig. 3c. A second simulation (Evros_M4P) is performed using MODIS hot spots and the colocation with the MISR plumes is shown In Fig. 3d. The emission sources for this run are taken from the 09:10 UTC (12:10 PM local time) Terra overpass assuming that the fire intensity remains constant throughout the simulation period. This assumption imposes several limitations to the description of smoke emissions because the fires typically grow in strength during morning and noon hours as the

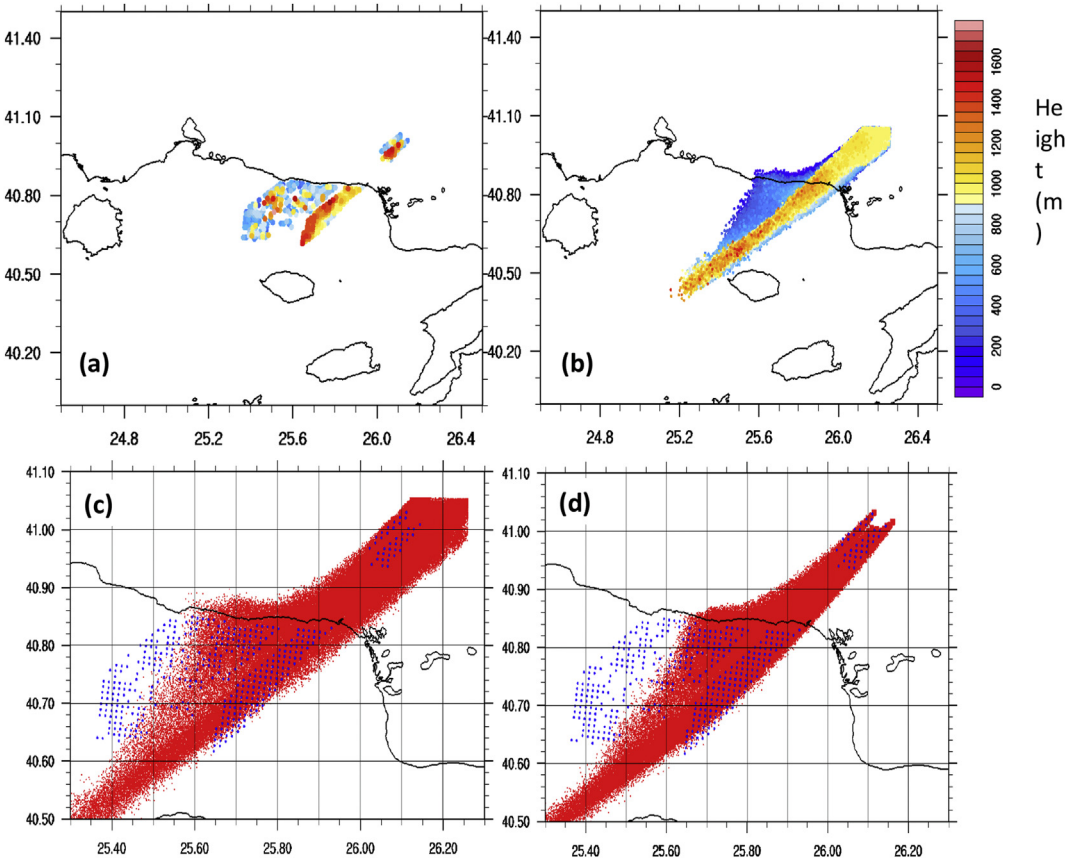

Fig. 3. Smoke plume heights (m) a) as observed from MISR (MINX sampling at 1 × 1 km resolution) b) Evros_S4P simulation. c) Colocation of MISR smoke detections (blue dots) with Evros_S4P smoke plumes. d) Colocation of MISR smoke detections (blue dots) with Evros_M4P (red) smoke plumes, 25 August 2011, 09:10 UTC. (For interpretation of the references to color in this figure legend, the reader is referred to the web version of this article.)

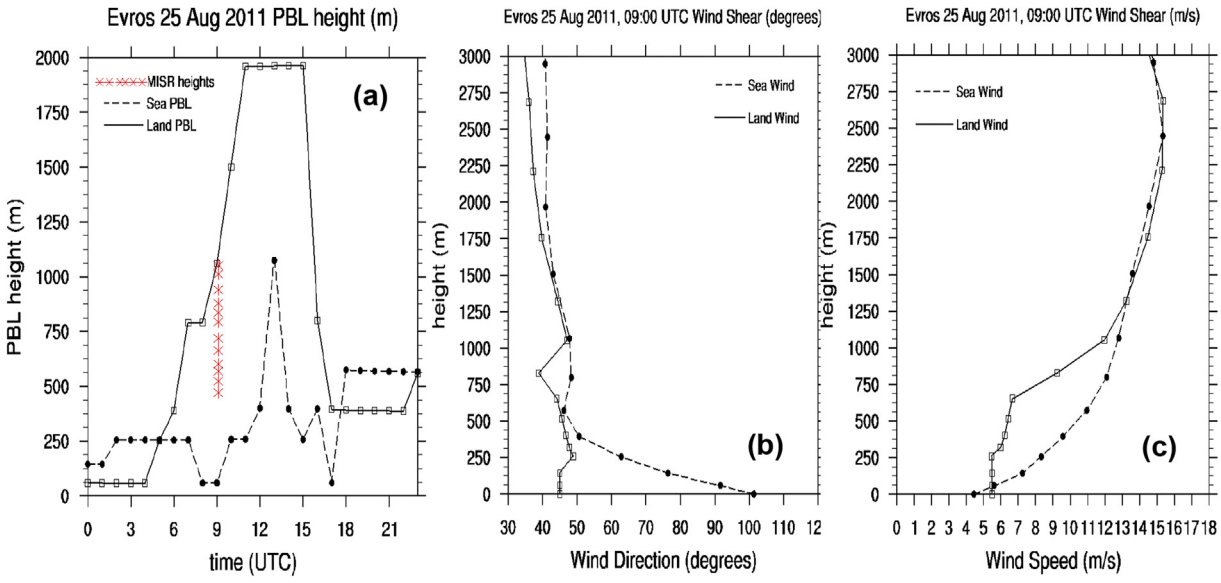

Fig. 4. a) Modeled PBL height close to the fire hot spots (Land PBL), off the coast (Sea PBL) and MISR observed smoke heights over the emission sources; b) Modeled vertical profiles of wind direction (degrees) near the sources (Land Wind) and off the coast (Sea Wind); c) Modeled vertical profiles of sea and land wind speed (m s^{-1}).

atmosphere warms up, the BL depth increases and winds are in general more intense. For example, as seen in Fig. 4a, surface heating during the morning and noon results in a significant diurnal variation of almost 2 km in the planetary boundary layer height (PBLH). The night and early morning PBLH in the WRF model are below 100 m, whereas during 11:00–15:00 UTC PBLH grows up to 2 km over land. At the time of MISR overpass (09:10 UTC) the observations of smoke elevation just over the fire areas (i.e. the plume rise) suggest that all observed smoke particles are within the modeled PBL (red (in the web version) markers in Fig. 4a). Over the sea, the PBLH remains well below 300–400 m (with the exception of 13:00 UTC), so that smoke particles moving from land towards the sea actually cross the PBL over the coastline and continue traveling in the free troposphere. Wind properties over sea and land are also different. Over the land, the modeled wind direction is almost constant (40°–50°) from the surface up to 3 km (Fig. 4b) while over the sea the wind gradually veers from 100° near the surface to 45° at 500 m height. Because of that, as soon as the smoke crosses the coastline, the lower parts of the plumes are shifted towards the west while the smoke that is lifted above 500 m continuous traveling SW. This explains the west divergence of the plume that is seen in Fig. 3. Moreover, the modeled wind speed from the surface up to 1 km is almost twice as high over sea than over land (Fig. 4c) thus enhancing the dispersion of smoke over the sea.

In order to test also the effects of the online calculation of smoke injection heights in smoke dispersion, an additional simulation is performed enabling the Freitas plume rise scheme. This run is performed using MODIS hot spots and FRP observations (Evros_M4F). The reason for this is that although the FireHub system is primarily designed to run with SEVIRI observations, a SEVIRI FRP algorithm is not yet available for operational use. This simulation results in underprediction of the smoke heights as seen in Fig. 5 and both plumes travel towards the west parallel to the coastline. This is probably due to the relatively low MODIS FRP values for this case and indicates the need for further optimization of the plume rise parameterization for local studies.

A comparison between the two simulations (Evros_M4P and Evros_S4P) and MISR observations is conducted using a discrete statistics methodology as described in Wilks (2006). According to

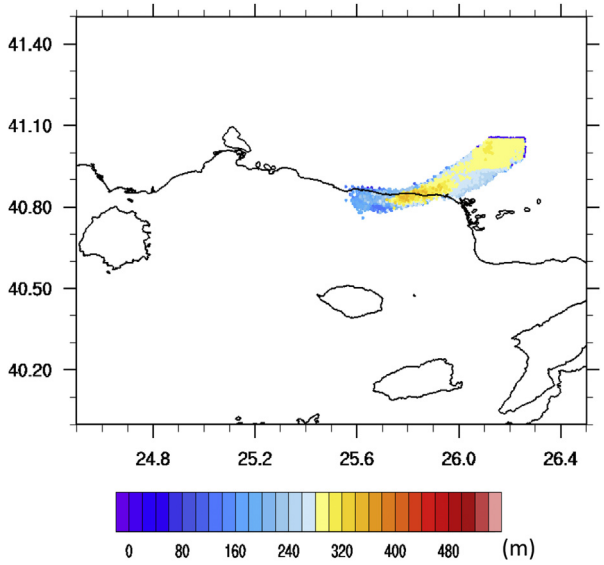

Fig. 5. Smoke dispersion from the Evros_M4F simulation (plume rise scheme), 25 August 2011, 09:10 UTC.

this methodology, data are first spatially collocated and then compared with regards to their different properties (smoke height, concentration, etc.). In particular, we firstly divide the modeling domain into 0.1° × 0.1° cells (as seen in Fig. 3c, d). For each cell, we extract the median smoke heights from MINX and from each model run. When a cell includes both observed and simulated smoke this is considered as hit (H). When smoke is observed but not simulated, the cell is characterized as a miss (M) and when smoke is simulated but not observed the cell is characterized as false alarm (F). The numbers of hits, misses and false alarms for each run are presented in Table 2. The score percentages in this table are calculated as follows: F% = F/(F + H + M), H% = H/(F + H + M), M% = M/(F + H + M). Basic statistics from the comparison between modeled and MISR median smoke heights are extracted only for the hit cells and are also presented in Table 2. Overall, Evros_S4P scored equal

Table 2
Statistical metrics from the comparison between FLEXPART-WRF and MISR smoke heights. Score percentages are shown in parenthesis.

	False (%)	Hits (%)	Miss (%)	R	RMSE (m)	BIAS (m)
Evros_S4P	21 (50%)	21 (50%)	0 (0%)	0.72	526.09	−502.30
Evros_M4P	8 (28%)	16 (55%)	5 (17%)	0.60	610.49	−592.38
Evros_M4F	6 (22%)	11 (41%)	10 (37%)	0.50	768.21	−750.09
Agion_Oros_S4P	193 (69%)	86 (31%)	0 (0%)	0.47	1135.89	−759.64
Agion_Oros_S4P 0–2.5 km				0.69	676.79	−575.53
Agion_Oros_M4F	112 (56%)	63 (32%)	23 (12%)	0.65	1157.25	−963.90
Agion_Oros_M4F 0–2.5 km				0.64	738.06	−667.98
Agion_Oros_S50P	115 (58%)	70 (35%)	15 (7%)	0.55	1100.21	−840.16
Peloponnese_S4P	243 (44%)	222 (40%)	88 (16%)	0.05	898.13	−139.21
Peloponnese_S50P	513 (74%)	177 (26%)	0 (0%)	−0.16	1142.85	−721.30

number of false and hits (50%), whereas Evros_M4P scored also 17% of missed cells. The correlation coefficients for Evros_S4P and Evros_M4P are 0.72 and 0.60 respectively, while RMSE and biases for these runs indicate an underprediction of smoke heights that is within the 500 m accuracy of the MISR height retrievals. For the explicit plume rise model run (Evros_M4F), r = 0.5 whereas RMSE and bias are 768 m and −750 m respectively. These results, combined with visual inspection of both modeled and observed plumes, indicate the dominant role of local atmospheric conditions in determining the smoke plume transport. Accurate information on the emission properties is also important but the sensitivity of the simulations to assimilated MODIS or SEVIRI hot spots is limited.

In an attempt to quantify the effects of this event to local air quality, a smoke aerosol emission rate of 1.7 kg s^{-1} is calculated from Eq. (1) based on average observed FRP of 66.45 MW. Using these emissions for the Evros_S4P simulation, results in a maximum vertical column TPM concentration of 18 mg m^{-2} close to the fire (Fig. 6a). As the plumes reach the coastline the TPM load is dramatically reduced to less than 1.0 mg m^{-2}. The near surface concentration of smoke TPM over the sea is also very low (<1 μg m^{-3}) while over land and close to the fire hot spots the modeled surface concentration is up to 20 μg m^{-3} (Fig. 6b). In the vertical, most of the emitted PM is distributed up to 1 km near the fire while downwind the highest TPM concentrations are found between 200 and 300 m (Fig. 6c).

3.3. Case 2: complex meteorological conditions (Agion Oros, 9 August 2012)

This fire ignited at the north part of Mount Athos peninsula at 18 UTC on 8 August 2012 and lasted until 18 UTC, 9 August 2012. Due to morning cloudiness on 9 August, SEVIRI did not record any hot spots between 6 and 9 UTC. The MISR instrument overpass at 9:20 UTC captured two distinct areas of smoke plumes (Fig. 7a). The southern smoke plume first travels west over the Thermaikos Gulf and then shifts north towards the city of Thessaloniki. As long as the plume reaches the coastline (40.50°N, 22.90°E) convective activity in the area lifts the smoke to heights of up to 3 km. Then, the elevated part of the initial smoke plume travels back towards the east and over central Chalkidiki (40.40°–41.10°N, 23.00°–24.00° E). This pattern is well reproduced by the model (Fig. 7b), as indicated by the return flow of elevated (1500–3000 m) smoke over Central Chalkidiki and Lake Volvi. The model is in this case initialized with a uniform release of particles between 0 and 1000 m. As reported earlier, hot-spot observations were not available during 6–9 UTC. For this reason, the fires observed at 6 UTC are also used for the 6–7 UTC and 7–8 UTC intervals and the fires observed at 9 UTC are also used for the 8–9 UTC interval. The concurrent presence of clouds is evident in the visible Terra image (Fig. 7c) and some of these clouds are probably misinterpreted as elevated smoke (>2.5 km) by the MINX analysis of MISR observations.

This case study demonstrates the benefits of using higher resolution meteorological data instead of the standard ECMWF or GFS global datasets. In order to examine the sensitivity of the simulation towards atmospheric driving fields, we run the WRF model at a resolution of 50 × 50 km (e.g. similar to the global GFS model output) and we drive FLEXPART-WRF with the three-hourly (00, 03, 06, 09, 12, 15, 18, 21) WRF model outputs. As seen in Fig. 7d, this run fails to reproduce certain characteristics of the smoke dispersion; the particle heights remain below 1500 m, intense dispersion starts close to the source, and redirection of the smoke plume towards Thessaloniki over Thermaikos Gulf is not reproduced. Instead, the plume propagates further to the west reaching the opposite coastline.

Comparison of collocated MISR and FLEXPART-WRF smoke over a 0.1° × 0.1° grid (Fig. 8a) illustrates the better agreement between the model and observations for the high resolution run compared to the GFS-driven run (Fig. 8b). Enabling the plume rise scheme (Agion_Oros_M4F) also results in a good representation of the smoke plume, including the returning flow of elevated smoke, however with a divergence of several kilometers from the observed plume (Fig. 9). The statistical comparison between these runs is summarized in Table 2. Due to the rather complex situation that includes elevated smoke, convection and also cloud obscuration, a rather modest percentage of 31–32% hits is calculated and the RMSE of modeled versus observed smoke heights exceeds 1 km. These statistical metrics are significally improved when limiting the comparison to the height cluster 0–2.5 km (Table 2). The statistics for the low resolution run (Agion_Oros_S50P) are similar to the other runs keeping also in mind that this run scored more correct rejection cells. However, as seen previously in Fig. 7d, several characteristics of the smoke dispersion such as the north turn of the plume over Thermaikos Gulf and the elevated return flow over Chalkidiki have not been reproduced in the Agion_Oros_S50P run. This is also an indication that such model/satellite statistical comparisons need to be carefully evaluated and interpreted together with real images.

As seen from the visible MODIS channel in Fig. 7c and also from the high resolution (4 × 4 km) WRF run in Fig. 10a, convergence of moisture from the Aegean Sea results in deep convection and development of clouds that coexist with smoke particles. This situation is not reproduced in the corresponding GFS run (Fig. 10b). With regards to the PBL, Fig. 10c represents the complexity of the PBL pattern at 4 × 4 km which also cannot be reproduced in the low resolution simulation (Fig. 10d), thus affecting the modeling of smoke dispersion. The development of convective clouds in the vicinity of the smoke dispersion event results in increased vertical wind shear (Fig. 11). Convection starts at 08:00 UTC, and by 10:00

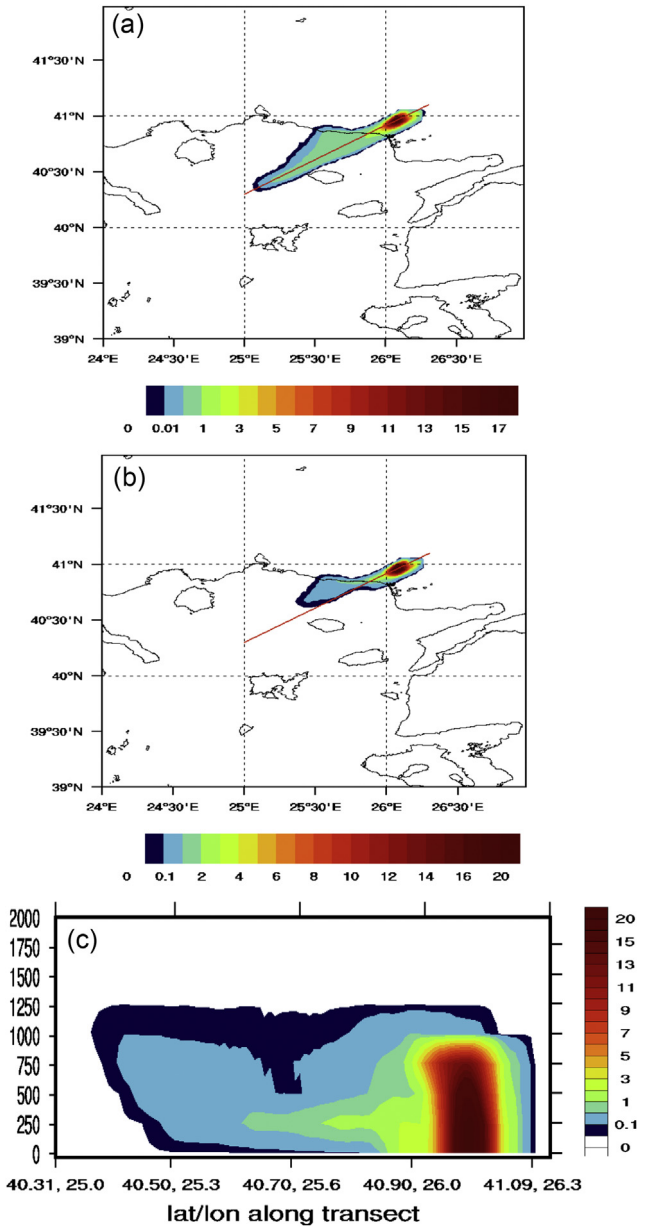

Fig. 6. a) Column concentration of modeled smoke TPM (mg m^{-2}). The red line indicates the location of the vertical cross-section shown in (c); b) Smoke TPM concentration (μg m^{-3}) at the first model layer; c) Vertical cross-section of TPM concentration (μg m^{-3}), 25 August 2011, 09:10 UTC. (For interpretation of the references to color in this figure legend, the reader is referred to the web version of this article.)

UTC the cloud top reaches 9 km height. The location of the vertical cross-section is indicated with a red line in the embedded topographic map plot in Fig. 11a. As a result of the convective activity, the easterly flow near the surface gradually veers to a westerly flow above 2 km height. Smoke is transported upward due to the convective updrafts and the particles that are elevated above 1500–1700 m continue traveling towards the east. These smoke plumes are evident at latitudes higher than 40.4° and east from 23° in both the MISR and model images. The interchange of heat fluxes between land and water bodies that is responsible for local-scale wind breezes and vertical winds cannot be adequately described in lower-resolution models. The fate of smoke plumes is heavily dependent on such local-scale circulations, thus emphasizing on the need to employ high-resolution meteorological forecasts in early warning systems like FireHub.

The intensity of this event is also depicted in the MODIS AOD that reaches up to 0.9 (Fig. 12a) with maximum values mainly over land. Assuming a smoke extinction coefficient (β_e) of 4.6 (m^2 g^{-1}) (e.g. Ichoku and Kaufman, 2005), an AOD value of 0.9 would imply a column TPM concentration (M_d) of 0.19 g m^{-2} (AOD = $\beta_e \times M_d$). Extending this consideration for a plume depth of 3 km, the average concentration of observed smoke TPM is estimated close to 65 μg m^3. Ofcourse, smoke is not uniformly distributed inside the traveling plumes and taking also into account the uncertainty regarding the smoke extinction coefficient value, such a computation provides only a rough estimation of the observed particle concentrations and no valid information about TMP concentrations at the various atmospheric levels. In order to estimate the TPM concentrations in the model, for an average MODIS FRP of 407 MW we use Eq. (1) and we calculate a TPM emission rate of 10.6 kg s^{-1}. Using this emission rate throughout the Agion_Oros_S4P simulation the concentrations of smoke TPM column reach 40 mg m^{-2} over the Thermaikos Gulf and 4 mg m^{-2} over the city of Thessaloniki. The corresponding modeled AOD pattern (Fig. 12b) is similar to MODIS although high values are also found over the sea. In the vertical, the base of the main (southern) plume is found to be at surface level (Fig. 13 top) but as seen in the other two cross-sections of Fig. 13 (along 40.35°N and 40.45°N) the plumes over land are detached from the surface. The modeled concentration of smoke TPM in the first model layer (0–250 m) exceeds 70 μg m^{-3} over several inhabited areas at Chalkidiki. However Thessaloniki is not directly affected by this episode since TPM remains well below 5 μg m^{-3} over the city area. This is also confirmed by the local air quality measurements that do not report any significant increase in fire-related tracers during this period.

3.4. Case 3: severe wildfire event (Peloponnese, 26 August 2007)

Devastating wildfires occurred during the period 25–27 August 2007 in Peloponnese. An analysis of MISR observations during this event is also presented by Liu et al. (2009). The synoptic conditions on 25 August 2007 are characterized by a high-pressure system over the central Mediterranean and a low-pressure system over Turkey. This combination resulted in sharp pressure gradients over the Aegean Sea and produced strong NE winds, with gusts exceeding 20 m s^{-1} at Peloponnese. High temperatures (>40 °C) and very low moisture levels over western Peloponnese during the previous days, favored the ignition of hazardous wildfires (Founda and Giannakopoulos, 2009; Athanasopoulou et al., 2014).

Due to the prevailing strong N–NE winds on August 26, smoke from these wildfires was transported towards the Central Mediterranean. The smoke plumes are observed from the Terra satellite, and their locations and heights are captured from the MISR instrument (Fig. 14a). Digitalization of MISR data with MINX software using a sampling rate of 1 × 1 km, indicates a SW advection of smoke plumes with heights ranging from 500 m to more than 3 km. Increased heights close to 3 km are found near the sources, and the elevation of the plumes gradually reduces to below 1.5 km downwind, with the exception of the southern plumes, where the smoke remains at 2.5–3 km for several kilometers away from the coast. Assuming a uniform release of particles between 0 and 1 km, the simulation of this event with FLEXPART-WRF (Peloponnese_S4P) indicates satisfactory agreement with MISR observations (Fig. 14b), also keeping in mind the complexity of the situation that incorporates a total of 11,033 hot-spot observations during the period 25 August 12:00 UTC – 26 August 12:00 UTC with FRP values reaching up to 6000 MW. Smoke originating from fires north of 38°N (Evoia) is also evident in the modeling results. Close to the

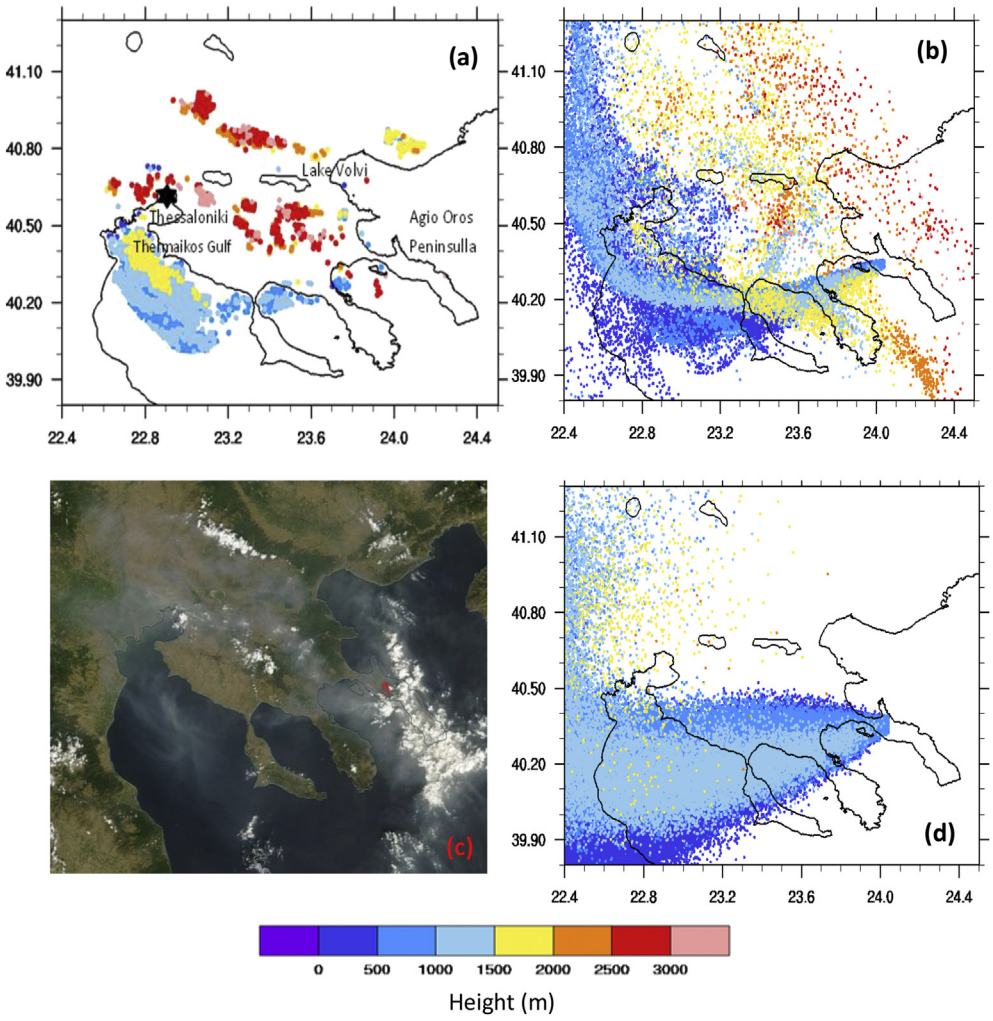

Fig. 7. a) Observation of smoke plume heights from MISR b) Simulated smoke plume heights from Agion_Oros_S4P c) Visual channel MODIS. The red spots indicate the location of the fire. d) Simulated smoke heights from Agion_Oros_S50P, 9 August 2012, 09:20 UTC. (For interpretation of the references to color in this figure legend, the reader is referred to the web version of this article.)

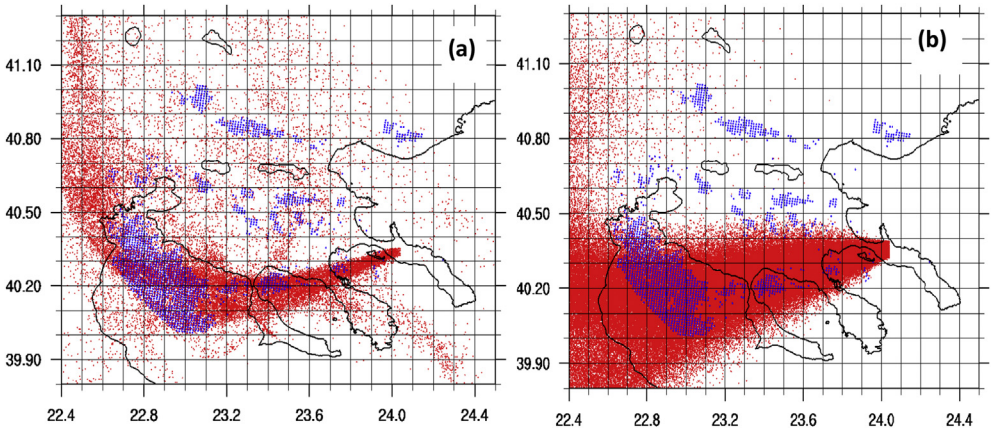

Fig. 8. a) MISR smoke detections (blue) and Agion_Oros_S4P particles (red) b) MISR particles (blue) and Agion_Oros_S50P particles (red), 9 August 2012, 09:20 UTC. (For interpretation of the references to color in this figure legend, the reader is referred to the web version of this article.)

sources and over the land the PBL is deeper and the simulated smoke particles are mixed up to a height of 2–2.5 km. As the plumes travel SW over the sea and into the free troposphere, the modeled smoke layer is further elevated exceeding 3 km height. In order to examine the sensitivity towards meteorological forcing one more simulation is performed (Peloponense_S50P) with the same emissions but this time FLEXPART-WRF is driven by the 3-hourly WRF outputs at 50 × 50 km resolution. The general

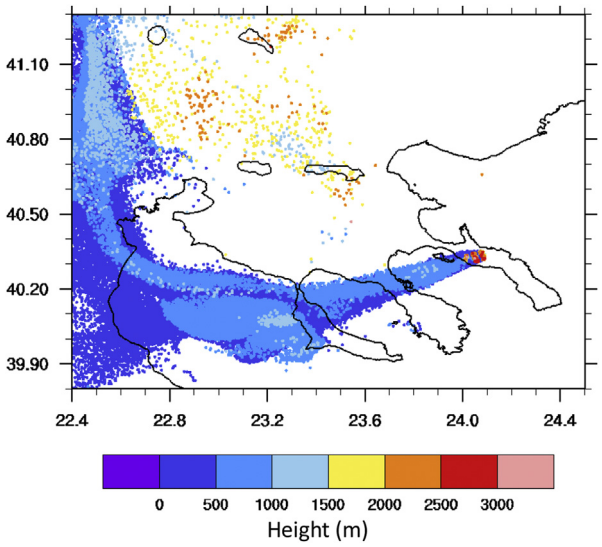

Fig. 9. Smoke heights from the Agion_Oros_M4F simulation (plume rise scheme), 9 August 2012, 09:20 UTC.

pattern of smoke dispersion is still reproduced in this run however with lower heights that in general do not exceed 2 km (Fig. 14c).

These simulations consist of sequential hourly runs starting on 25 August 2007, 12:00 UTC. In this way, the spatiotemporal variability of fire locations is continuously assimilated in the model and the smoke particles from the previous run are used as initial conditions for any subsequent simulation. The comparison between modeled smoke and MODIS observations on 25 and 26 of August (Fig. 15) reconfirms the SW long-range smoke transport over the sea. The average MODIS FRP during this event (25 and 26 of August) is 225 MW, and from Eq. (1) we estimate an average emission rate of 5.85 kg s^{-1}. Using this emission rate the column concentrations of smoke TPM near the sources exceed 300 mg m^{-2} on the 25th and 1500 mg m^{-2} on the 26th of August, respectively (Fig. 15b, d). Apart from the biomass fires in Peloponnese, significant amounts of smoke are also produced during the same period by wildfires at the island of Evoia. In-situ measurements from the air quality measuring network in Athens indicate a contribution of these fires to surface PM10 levels by 32 and 15 μg m^{-3} on the 25th and 26th of August respectively. The corresponding modeled TPM concentrations – averaged for the same stations – are 11 and 5 μg m^{-3} for these days. Although the concentrations are underpredicted the

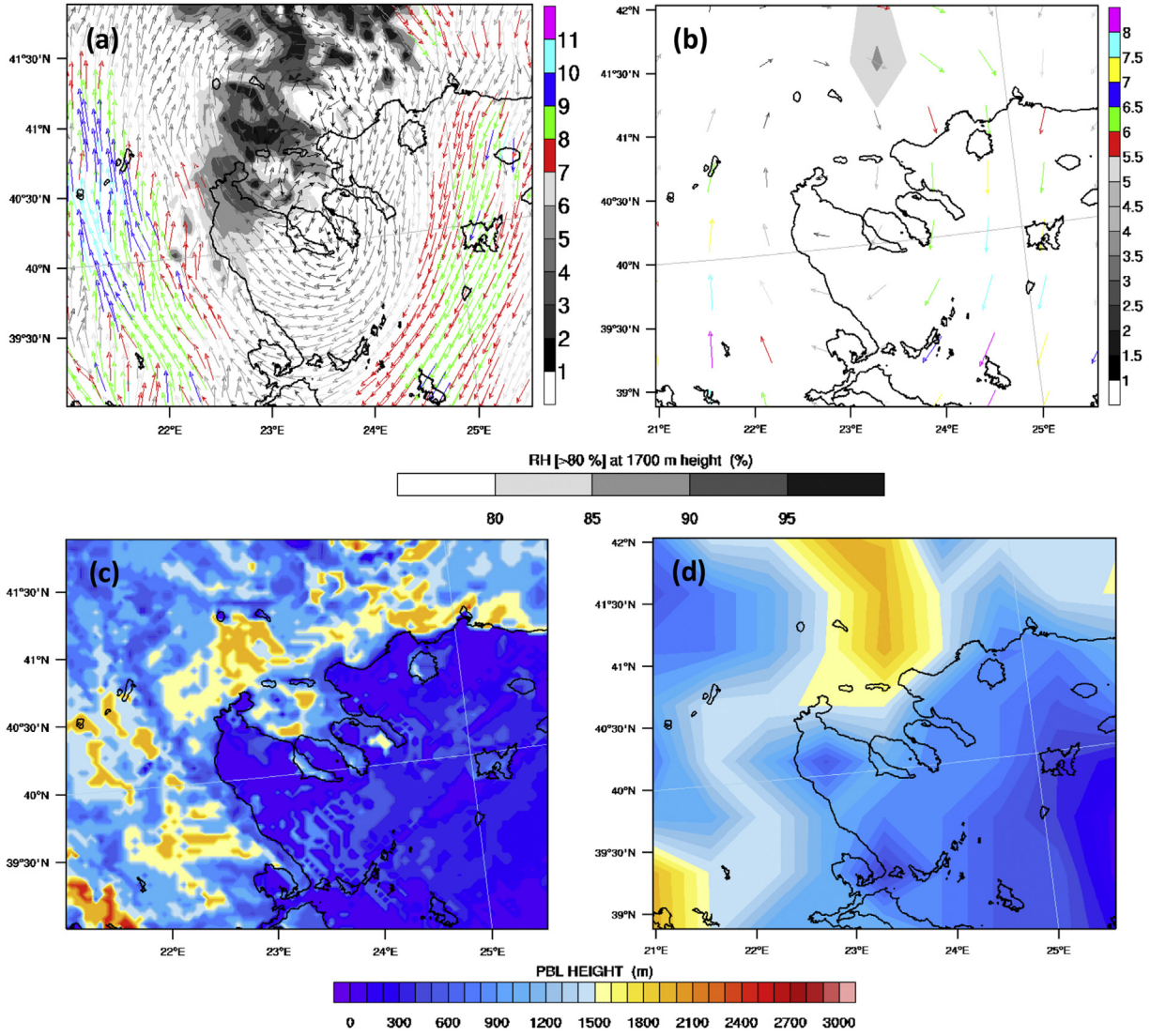

Fig. 10. a) Wind speed (m s^{-1}, color scaled vectors) and Relative Humidity >80% (i.e. clouds) at 1700 m height from the 4 × 4 km model run. b) Wind speed (m s^{-1}, color scaled vectors) and Relative Humidity >80% (i.e. clouds) from the 0.5° × 0.5° run (notice the different wind speed scale). c) PBL height from the 4 × 4 km model run. d) PBL height from the 0.5° × 0.5° model run, at 9 August 2012 09:00 UTC. (For interpretation of the references to color in this figure legend, the reader is referred to the web version of this article.)

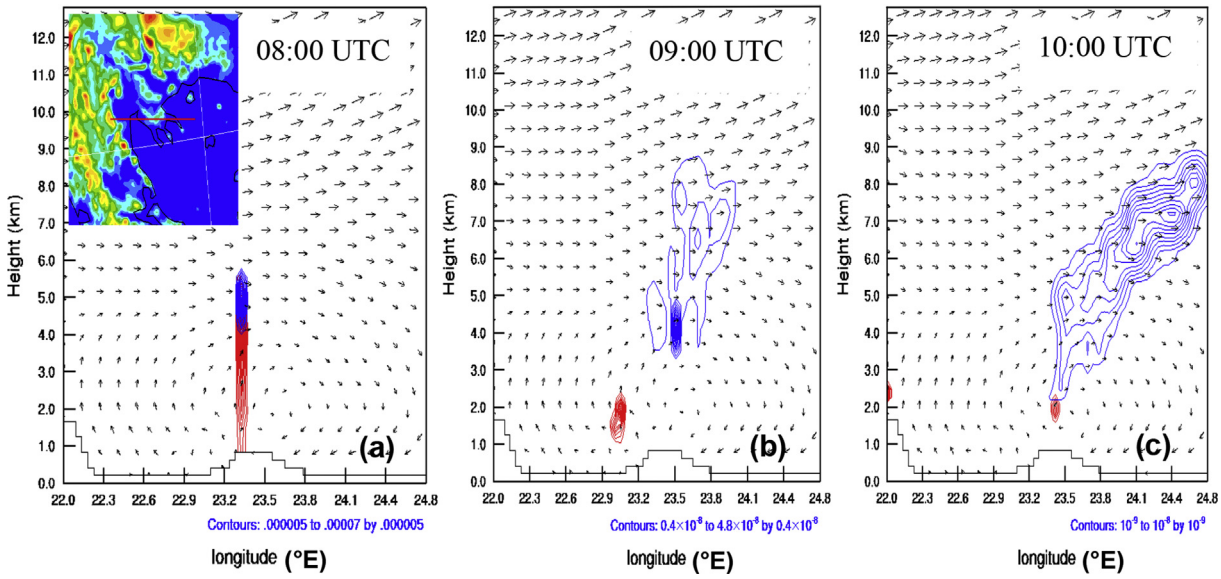

Fig. 11. Vertical cross-section of liquid condensates mixing ratio (red contours in g kg^{-1}), ice condensates mixing ratio (blue contours in g kg^{-1}) and wind vectors on 9 August 2012 a) 08:00 UTC; b) 09:00 UTC; c) 10:00 UTC. The red line in the embedded topographic map of Fig. 11a indicates the location of the cross-section. (For interpretation of the references to color in this figure legend, the reader is referred to the web version of this article.)

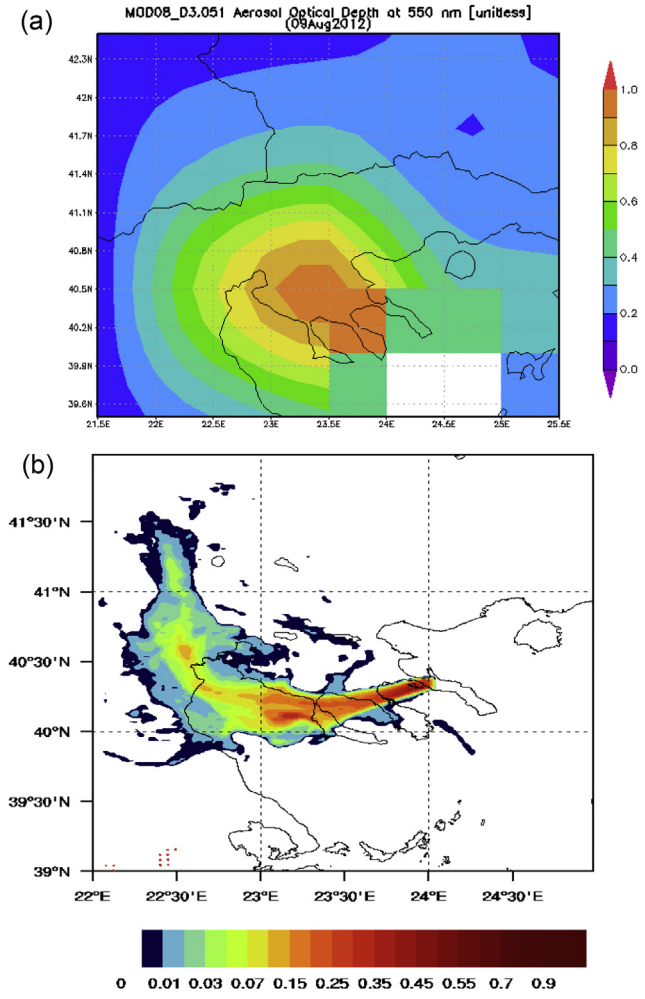

Fig. 12. a) MODIS AOD and b) Modeled smoke AOD from the Agion_Oros_S4P simulation, 9 August 2012, 09:20 UTC.

observed 2:1 ratio between 25 and 26 of August is still reproduced in the model. Taking into account that the emission rate is kept constant throughout the simulation it seems that the hourly update of SEVIRI hot spots somehow compensates for the implicit emissions.

4. Conclusions and discussion

A synergistic satellite/modeling approach, driven by geostationary observations from the MSG/SEVIRI instrument, is utilized in this study, in order to demonstrate the first steps towards the development of a high-resolution smoke forecasting system and identify the specific mechanisms that govern smoke dispersion over particularly complex surfaces such as South Europe and especially Greece. A top-down approach is adopted and satellite observations of fire hot spots and intensity (FRP) are used to drive the smoke dispersion simulations. The analysis of three case studies with unique characteristics indicates the complexity of smoke dispersion patterns and the uncertainties associated with the description and forecasting of similar events. This uncertainty can be decomposed in the two main factors related to the main model inputs i) Meteorological driver and ii) Satellite fire information.

Analysis of the first case study involves a relatively simple weather pattern with spatially constrained fire emission sources. In such cases, the interchange from a deeper PBL over land to a shallower PBL over the sea leads in decoupling of smoke layers aloft from the surface into the free troposphere and favors long-range transport over the sea. This abrupt change between land and sea PBL, that is typical for a coastal environment such as Greece, may also explain the frequent occurrence of several similar smoke plume episodes after just medium or even low intensity fires. In the case of convective activity over a complex coastline – like the one described in the second fire episode - the simulations clearly benefit from the improvements in the resolution and detail of the atmospheric model. Several driving forces such as terrain variability and PBL heights are better represented in FLEXPART-WRF and the model is capable of resolving local features of smoke dispersion. The importance of the continuous geostationary information as provided by MSG/SEVIRI through the FireHub platform

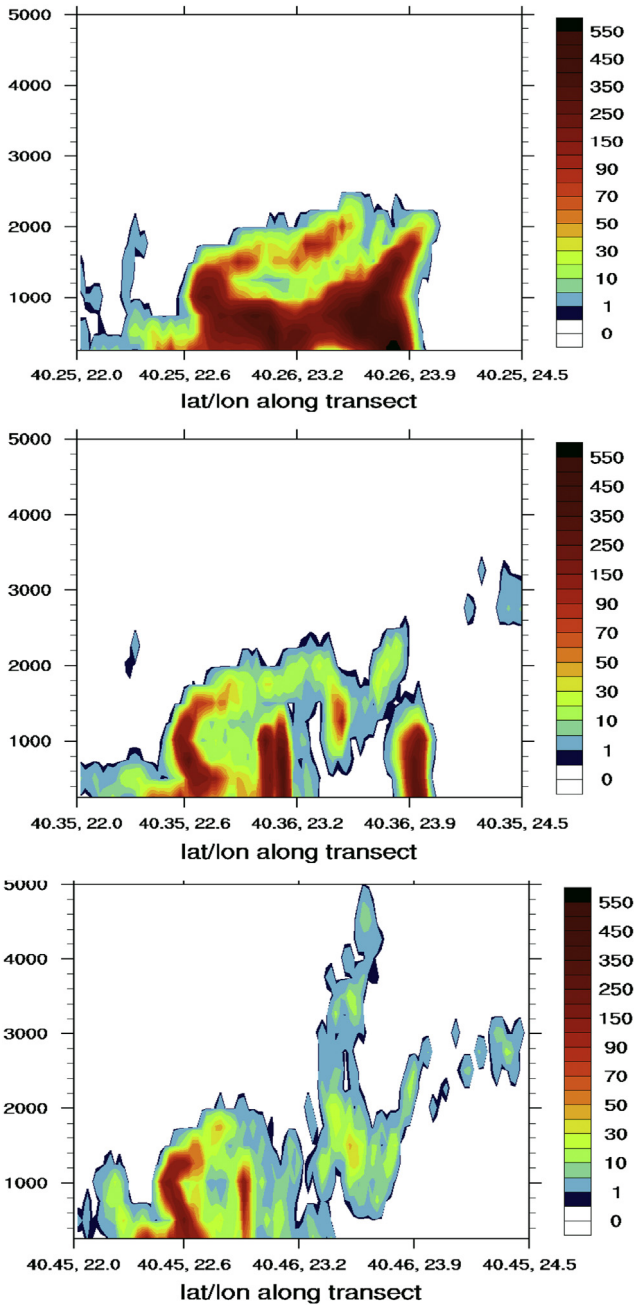

Fig. 13. Vertical cross sections of smoke TPM concentration (μg m^{-3}) along 40.25N latitude (up) 40.35N (middle) and 40.45N (down), from the Agion_Oros_S4P simulation, 9 August 2012, 09:20 UTC.

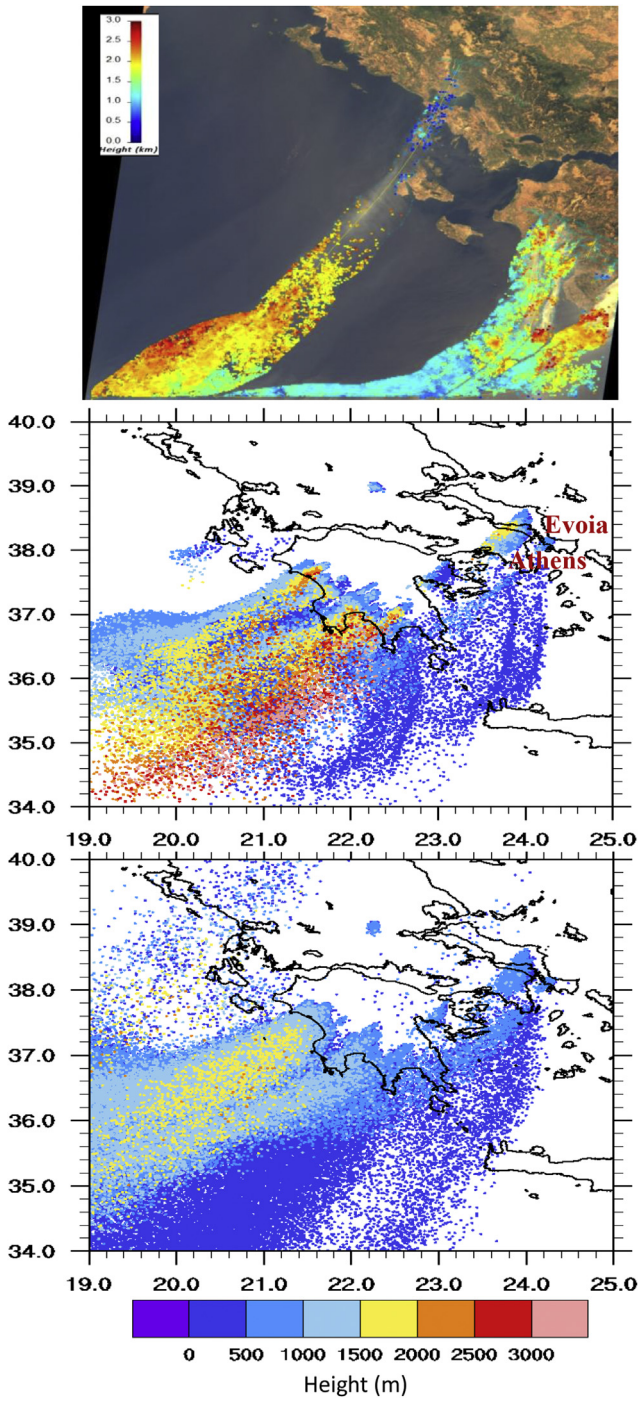

Fig. 14. Smoke plume heights on 26 August 2007, 09:30 UTC. MISR observations (upper); Peloponense_S4P simulation (middle); Peloponense_S50P simulation (lower).

becomes more evident for fires events like the 2007 case described here, that are characterized by long duration and greatly varying intensity. Such information cannot be retrieved from polar-orbiting instruments alone, thus affecting the quality of smoke dispersion forecasts, especially for situations when real-time emergency response is required. The evaluation of smoke plume geometries with MISR stereo-heights is found to be a valuable tool for assessing the model performance, however this approach is also proven to suffer from certain limitations, as for example when the satellite swath is narrower than the plume itself (e.g. the case of Peloponnese fires) or when several parts of the plume are not observed due to cloudiness (e.g. the Agion Oros case). In most cases, visual comparison between real images and modeled plumes is necessary to assess the model's performance in excess to statistical approaches.

The simulated and measured surface concentrations away from the fire sources reveal high contents of smoke aerosol particles, exceeding the EU threshold values. In many instances these high concentrations affect residential areas and raise certain worries about the impact of smoke plumes from fires on population exposure and health. Even though the absolute concentrations strongly depend on the smoke emission rates, which is in turn calculated by observed FRPs and include certain assumptions, it is quite important for operational use of smoke dispersion to be able

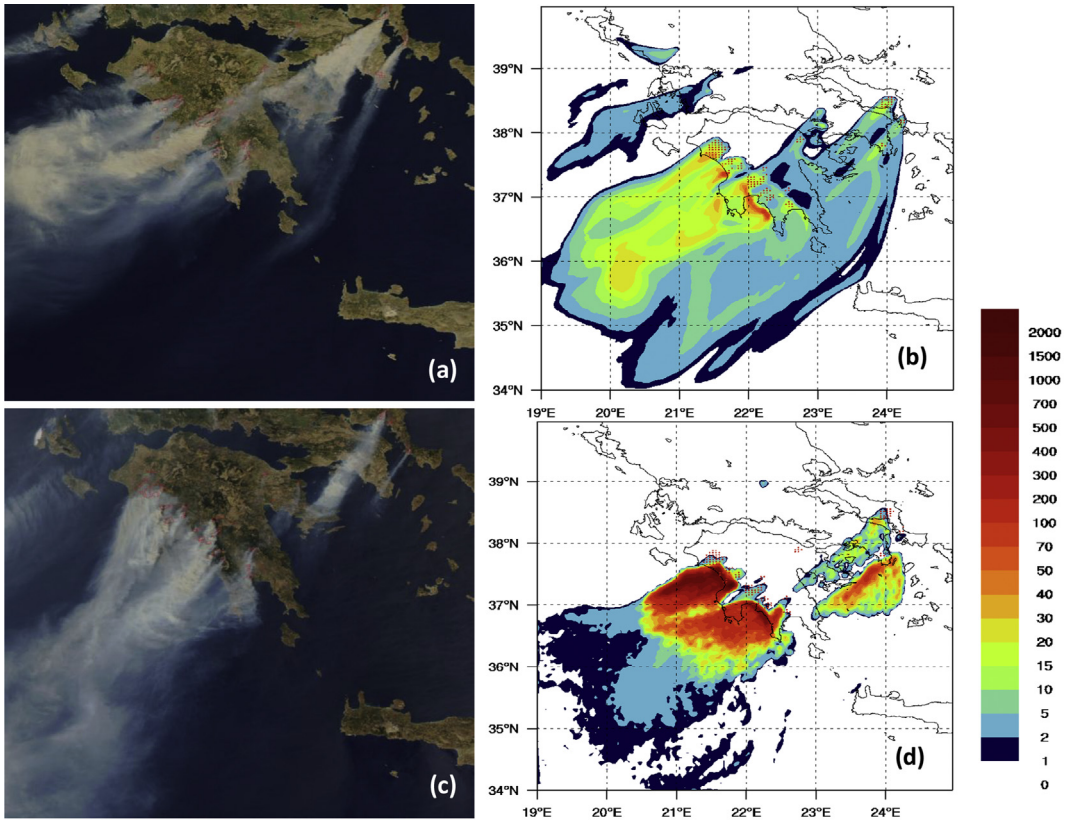

Fig. 15. a) MODIS image on 25 August 2007 20:00 UTC; b) Column concentration of smoke TPM (mg m^{-2}) from the Peloponnese_S4P simulation, 25 August 2007 20:00 UTC; c) MODIS image on 26 August 2007 09:30 UTC; d) Column concentration of smoke TPM (mg m^{-2}) from the Peloponnese_S4P simulation, 26 August 2007 09:30 UTC. Red dots indicate the SEVIRI hot spots that were detected on 25 and 26 of August 2007. (For interpretation of the references to color in this figure legend, the reader is referred to the web version of this article.)

to forecast the most accurate in space and time evolution of a smoke plume nearby residential areas. The emission rates for the total smoke particulate matter in this study have been estimated from the MODIS FRP based on a top-down approach proposed by Ichoku and Ellison (2014). On-line assimilation of SEVIRI FRP is not yet available for forecasting applications. A corresponding retrieval algorithm will be implemented in a forthcoming operational version of the system in order to link the observed fire intensity with model emission rates and injection heights. Future plans for the improvement of smoke dispersion modeling also include the further development and optimization of the plume-rise scheme in FLEXPART-WRF, incorporating both SEVIRI FRP observations and WRF meteorological fields. Linking of space-borne observations with fire physical processes is important for avoiding unnecessary assumptions and will allow the determination of case-specific emission rates for each fire spot in real time.

Moreover, the physical processes that govern forest fires are actually much more complex, and several components are still missing or not fully understood. For example, the atmospheric conditions in the vicinity of severe fires are also affected by the fire itself (e.g. pyroconvection, smoke radiative effects, activation of smoke as CCN, IN etc.). These interactions must also be included in atmospheric models for climate change considerations. Application of such integrated modeling and satellite methodologies for sub-Sahel Africa and Amazonia could improve our understanding on the impacts of major sources in global biomass burning.

Acknowledgments

The publication was supported by the European Union Seventh Framework Programme (FP7-REGPOT-2012-2013-1), in the framework of the project BEYOND, under Grant Agreement No. 316210 (BEYOND – Building Capacity for a Centre of Excellence for EO-based monitoring of Natural Disasters, http://ocean.space.noa.gr/BEYONDsite). MISR plume-height data were obtained with the MINX code, with MISR data obtained from the NASA Langley Atmospheric Sciences Data Center (http://eosweb.larc.nasa.gov). http://misr.jpl.nasa.gov/getData/accessData/MisrMinxPlumes/index.cfm.

References

Amiridis, V., Balis, D.S., Giannakaki, E., Stohl, A., Kazadzis, S., Koukouli, M.E., Zanis, P., 2009. Optical characteristics of biomass burning aerosols over Southeastern Europe determined from UV-Raman lidar measurements. Atmos. Chem. Phys. 9, 2431–2440. http://dx.doi.org/10.5194/acp-9-2431-2009.

Amiridis, V., Giannakaki, E., Balis, D.S., Gerasopoulos, E., Pytharoulis, I., Zanis, P., Kazadzis, S., Melas, D., Zerefos, C., 2010. Smoke injection heights from agricultural burning in Eastern Europe as seen by CALIPSO. Atmos. Chem. Phys. 10, 11567–11576.

Amiridis, V., Zerefos, C., Kazadzis, S., Gerasopoulos, E., Eleftheratos, K., Vrekoussis, M., Stohl, A., Mamouri, R.E., Kokkalis, P., Papayannis, A., Eleftheriadis, K., Diapouli, E., Keramitsoglou, I., Kontoes, C., Kotroni, V., Lagouvardos, K., Marinou, E., Giannakaki, E., Kostopoulou, E., Giannakopoulos, C., Richter, A., Burrows, J.P., Mihalopoulos, N., 2012. Impact of the 2009 Attica wild fires on the air quality in urban Athens. Atmos. Environ. 46, 536–544.

Andreae, M.O., 1993. The influence of tropical biomass burning on climate and the atmospheric environment. In: Oremland, R.S. (Ed.), Biogeochemistry of Global Change: Radiatively Active Trace Gases. Chapman and Hall, New York, pp. 113–150.

Andreae, M.O., Merlet, P., 2001. Emission of trace gases and aerosols from biomass burning. Glob. Biogeochem. Cycles 15, 955–966, 2001.

Athanasopoulou, E., Rieger, D., Walter, C., Vogel, H., Karali, A., Hatzaki, M., Gerasopoulos, E., Vogel, B., Giannakopoulos, C., Gratsea, M., Roussos, A., 2014. Fire risk, atmospheric chemistry and radiative forcing assessment of wild fires

in eastern Mediterranean. Atmos. Environ. 95, 113–125. http://dx.doi.org/10.1016/j.atmosenv.2014.05.077.
Brioude, J., Cooper, O.R., Feingold, G., Trainer, M., Freitas, S.R., Kowal, D., Ayers, J.K., Prins, E., Minnis, P., McKeen, S.A., Frost, G.J., Hsie, E.-Y., 2009. Effect of biomass burning on marine stratocumulus clouds off the California coast. Atmos. Chem. Phys. 9, 8841–8856.
Brioude, J., Arnold, D., Stohl, A., Cassiani, M., Morton, D., Seibert, P., Angevine, W., Evan, S., Dingwell, A., Fast, J.D., Easter, R.C., Pisso, I., Burkhart, J., Wotawa, G., 2013. The Lagrangian particle dispersion model FLEXPART-WRF version 3.1. Geosci. Model. Dev. 6, 1889–1904. http://dx.doi.org/10.5194/gmd-6-1889-2013.
Colarco, P.R., Schoeberl, M.R., Doddridge, B.G., Marufu, L.T., Torres, O., Welton, E.J., 2004. Transport of smoke from Canadian forest fires to the surface near Washington, D.C.: injection height, entrainment, and optical properties. J. Geophys. Res. 109, D06203. http://dx.doi.org/10.1029/2003JD004248, 2004.
Forster, C., Wandinger, U., Wotawa, G., James, P., Mattis, I., Althausen, D., Simmonds, P., O'Doherty, S., Jennings, S., Kleefeld, C., Schnieder, J., Trickl, T., Kreipl, S., Jager, H., Stohl, A., 2001. Transport of boreal forest fire emissions from Canada to Europe. J. Geophys. Res. 106, 22 887–22 906.
Founda, D., Giannakopoulos, C., 2009. The exceptionally hot summer of 2007 in Athens, 306 Greece, a typical summer in the future climate? Glob. Planet. Change 67, 227–236.
Freeborn, P.H., Wooster, M.J., Hao, W.M., Ryan, C.A., Nordgren, B.L., Baker, S.P., Ichoku, C., 2008. Relationships between energy release, fuel mass loss, and trace gas and aerosol emissions during laboratory biomass fires. J. Geophys. Res. 113, D01301. http://dx.doi.org/10.1029/2007JD008679.
Freitas, S.R., Longo, K.M., Chatfield, R., Latham, D., Silva Dias, M.A.F., Andreae, M.O., Prins, E., Santos, J.C., Gielow, R., Carvalho Jr., J.A., 2007. Including the sub-grid scale plume rise of vegetation fires in low resolution atmospheric transport models. Atmos. Chem. Phys. 7, 3385–3398.
IPCC, 2014. In: Field, C.B., Barros, V.R., Dokken, D.J., Mach, K.J., Mastrandrea, M.D., Bilir, T.E., Chatterjee, M., Ebi, K.L., Estrada, Y.O., Genova, R.C., Girma, B., Kissel, E.S., Levy, A.N., MacCracken, S., Mastrandrea, P.R., White, L.L. (Eds.), Climate Change 2014: Impacts, Adaptation, and Vulnerability. Part A: Global and Sectoral Aspects. Contribution of Working Group II to the Fifth Assessment Report of the Intergovernmental Panel on Climate Change. Cambridge University Press, Cambridge, United Kingdom and New York, NY, USA, p. 1132, 2014.
Ichoku, C., Kaufman, Y.J., 2005. A method to derive smoke emission rates from MODIS fire radiative energy measurements. IEEE Trans. Geosci. Remote Sens. 43 (11), 2636–2649. http://dx.doi.org/10.1109/TGRS.2005.857328, 2005.
Ichoku, C., Ellison, L., 2014. Global top-down smoke-aerosol emissions estimation using satellite fire radiative power measurements. Atmos. Chem. Phys. 14, 6643–6667. http://dx.doi.org/10.5194/acp-14-6643-2014. www.atmos-chem-phys.net/14/6643/2014/.
Kahn, R.A., Li, W.-H., Moroney, C., Diner, D.J., Martonchik, J.V., Fishbein, E., 2007. Aerosol source plume physical characteristics from space-based multiangle imaging. J. Geophys. Res. 112, D11205,. http://dx.doi.org/10.1029/2006JD007647.
Kelha, V., Rauste, Y., Hame, T., Sephton, T., Buongiorno, A., Frauenberger, O., Soini, K., Venalainen, A., San Miguel-Ayanz, J., Vainio, T., 2003. Combining AVHRR and ATSR satellite sensor data for operational boreal forest fire detection. Int. J. Remote Sens. 24 (8), 1691–1708.
Keramitsoglou, I., Kiranoudis, C.T., Sifakis, N., 2004. A multidisciplinary decision support system for forest fire crisis management. Environ. Manag. 33, 212–225.
Kontoes, C., Papoutsis, I., Herekakis, T., Sifakis, N., 2013. Wildfire Rapid Detection and Mapping and Post-fire Damage Assessment in Greece. In: Earthzine.
Langmann, B., Duncan, B., Textor, C., Trentmann, J., van der Werf, G.R., 2009. Vegetation fire emissions and their impact on air pollution and climate. Atmos. Environ. 43, 107–116, 2009.
Liu, Y., Kahn, R.A., Chaloulakou, A., Koutrakis, P., 2009. Analysis of the impact of the forest fires in August 2007 on air quality of Athens using multi-sensor aerosol remote sensing data, meteorology and surface observations. Atmos. Environ. http://dx.doi.org/10.1016/j.atmosenv.2009.04.010, 2009.
Myhre, G., Shindell, D., Breon, F.-M., Collins, W., Fuglestvedt, J., Huang, J., Koch, D., Lamarque, J.-F., Lee, D., Mendoza, B., Nakajima, T., Robock, A., Stephens, G., Takemura, T., Zhang, H., 2013. Anthropogenic and natural radiative forcing. In: Stocker, T.F., Qin, D., Plattner, G.-K., Tignor, M., Allen, S.K., Boschung, J., Nauels, A., Xia, Y., Bex, V., Midgley, P.M. (Eds.), Climate Change 2013: the Physical Science Basis. Contribution of Working Group I to the Fifth Assessment Report of the Intergovernmental Panel on Climate Change. Cambridge University Press, Cambridge, United Kingdom and New York, NY, USA., 2013.
Nelson, D., Averill, C., Boland, S., Morford, R., Garay, M., Thompson, C., Hall, J., Diner, D., Camphell, H., 2008. MISR Interactive eXplorer (MINX) v1.0 User's Guide. Jet Propulsion Lab, NASA. Published on the web. https://www.openchannelsoftware.com/projects/MINX.
Nelson, D.L., Garay, M.J., Kahn, R.A., Dunst, B.A., 2013. Stereoscopic height and wind retrievals for aerosol plumes with the MISR INteractive eXplorer (MINX). Remote Sens. 5, 4593–4628. http://dx.doi.org/10.3390/rs5094593, 2013.
Nenes, A., Seinfeld, J.H., 2003. Parameterization of cloud droplet formation in global climate models. J. Geophys. Res. 108 (D14), 4415. http://dx.doi.org/10.1029/2002JD002911.
Petrenko, M., Kahn, R.A., Chin, M., Soja, A., Kucsera, T., Harshvardhan, 2012. The use of satellite-measured aerosol optical depth to constrain biomass burning emissions source strength in a global aerosol model (GOCART). J. Geophys. Res. 117 (D18), D18212. http://dx.doi.org/10.1029/2012JD017870, 2012.
Randerson, J.T., Liu, H., Flanner, M.G., Chambers, S.D., Jin, Y., Hess, P.G., Pfister, G., Mack, M.C., Treseder, K.K., Welp, L.R., Chapin, F.S., Harden, J.W., Goulden, M.L., Lyons, E., Neff, J.C., Schuur, E.A.G., Zender, C.S., 2006. The impact of boreal Forest fire on climate warming. Science. http://dx.doi.org/10.1126/science.1132075.
Saide, P.E., Spak, S.N., Pierce, R.B., Otkin, J.A., Schaack, T.K., Heidinger, A.K., da Silva, A.M., Kacenelenbogen, M., Redemann, J., Carmichael, G.R., 2015. Central American Biomass Burning Smoke Can Increase Tornado Severity in the U.S.GRL doi: 0.1002/2014GL062826.
Sifakis, N.I., Iossifidis, C., Kontoes, C., Keramitsoglou, I., 2011. Wildfire detection and tracking over Greece using MSG-SEVIRI satellite data. Remote Sens. 3, 524–538, 2011.
Skamarock, W.C., Klemp, J.B., Dudhia, J., Gill, D.O., Barker, D.M., Duda, M.G., Huang, X.-Y., Wang, W., Powers, J.G., 2008. A Description of the Advanced Research WRF Version 3. In: NCAR Technical Note 475, 2008. http://www.mmm.ucar.edu/wrf/users/docs/arw_v3.pdf.
Sofiev, M., Siljamo, P., Valkama, I., Ilvonen, M., Kukkonen, J., 2006. A dispersion modelling system SILAM and its evaluation against ETEX data. Atmos. Environ. 40, 674–685. http://dx.doi.org/10.1016/j.atmosenv.2005.09.069.
Sofiev, M., Vankevich, R., Lotjonen, M., Prank, M., Petukhov, V., Ermakova, T., Koskinen, J., Kukkonen, J., 2009. An operational system for the assimilation of the satellite information on wild-land fires for the needs of air quality modelling and forecasting. Atmos. Chem. Phys. 9, 6833–6847.
Stohl, A., Berg, T., Burkhart, J.F., Fjæraa, A.M., Forster, C., Herber, A., Hov, O., Lunder, C., McMillan, W.W., Oltmans, S., Shiobara, M., Simpson, D., Solberg, S., Stebel, K., Strom, J., Torseth, K., Treffeisen, R., Virkkunen, K., Yttri, K.E., 2007. Arctic smoke – record high air pollution levels in the European Arctic due to agricultural fires in Eastern Europe in spring 2006. Atmos. Chem. Phys. 7, 511–534. http://dx.doi.org/10.5194/acp-7-511-2007.
Tyrlis, E., Lelieveld, J., 2013. Climatology and dynamics of the summer Etesian winds over the Eastern Mediterranean. J. Atmos. Sci. http://dx.doi.org/10.1175/JAS-D-13-035.1.
Val Martin, M., Logan, J.A., Kahn, R.A., Leung, F.-Y., Nelson, D.L., Diner, D.J., 2010. Smoke injection heights from fires in North America: analysis of 5 years of satellite observations. Atmos. Chem. Phys. 10, 1491–1510.
Val Martin, M., Kahn, R.A., Logan, J.A., Paugam, R., Wooster, M., Ichoku, C., 2012. Space-based observations constraints for 1-D plume-rise models. J. Geophys. Res. 117, D22204. http://dx.doi.org/10.1029/2012JD018370.
Wilks, D.S., 2006. Statistical Methods in the Atmospheric Sciences. Academic Press NY, pp. 260–271.
Wooster, M.J., Roberts, G., Perry, G.L.W., Kaufman, Y.J., 2005. Retrieval of biomass combustion rates and totals from fire radiative power observations: FRP derivation and calibration relationships between biomass consumption and fire radiative energy release. J. Geophys. Res. 110, D24311. http://dx.doi.org/10.1029/2005JD006318.